USGS
science for a changing world

Quantifying and Qualifying USGS ShakeMap Uncertainty

By David J. Wald, Kuo-Wan Lin, and Vincent Quitoriano

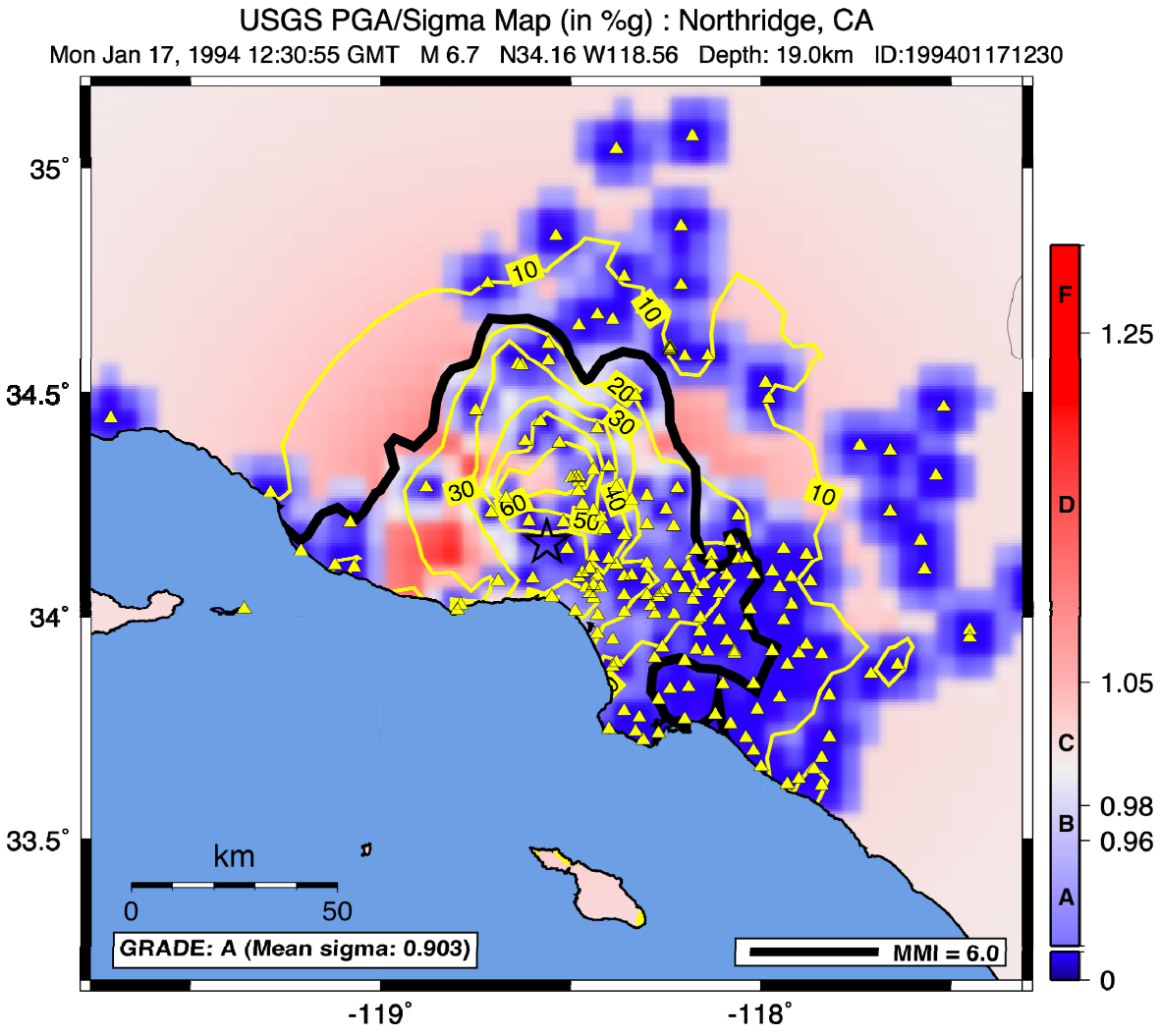

Open-File Report 2008-1238

U.S. Department of the Interior
U.S. Geological Survey

U.S. Department of the Interior
DIRK KEMPTHORNE, Secretary

U.S. Geological Survey
Mark D. Myers, Director

U.S. Geological Survey, Reston, Virginia 2008

For product and ordering information:
World Wide Web: http://www.usgs.gov/pubprod
Telephone: 1-888-ASK-USGS

For more information on the USGS—the Federal source for science about the Earth,
its natural and living resources, natural hazards, and the environment:
World Wide Web: http://www.usgs.gov
Telephone: 1-888-ASK-USGS

Suggested citation:
Wald, David J., Lin, Kuo-Wan, and Quitoriano, Vincent, 2008, Quantifying and Qualifying USGS ShakeMap Uncertainty: U.S. Geological Survey Open File Report 2008–1238

Contents

Quantifying and Qualifying USGS ShakeMap Uncertainty

By David J. Wald, Kuo-Wan Lin, and Vincent Quitoriano

Abstract

We describe algorithms for quantifying and qualifying uncertainties associated with USGS ShakeMap ground motions. The uncertainty values computed consist of latitude/longitude grid-based multiplicative factors that scale the standard deviation associated with the ground motion prediction equation (GMPE) used within the ShakeMap algorithm for estimating ground motions. The resulting grid-based "uncertainty map" is essential for evaluation of losses derived using ShakeMaps as the hazard input. For ShakeMap, ground motion uncertainty at any point is dominated by two main factors: (i) the influence of any proximal ground motion observations, and (ii) the uncertainty of estimating ground motions from the GMPE, most notably, elevated uncertainty due to initial, unconstrained source rupture geometry. The uncertainty is highest for larger magnitude earthquakes when source finiteness is not yet constrained and, hence, the distance to rupture is also uncertain. In addition to a spatially-dependant, quantitative assessment, many users may prefer a simple, qualitative grading for the entire ShakeMap. We developed a grading scale that allows one to quickly gauge the appropriate level of confidence when using rapidly produced ShakeMaps as part of the post-earthquake decision-making process or for qualitative assessments of archived or historical earthquake ShakeMaps. We describe an uncertainty letter grading ("A" through "F", for high to poor quality, respectively) based on the uncertainty map. A middle-range ("C") grade corresponds to a ShakeMap for a moderate-magnitude earthquake suitably represented with a point-source location. Lower grades “D” and “F” are assigned for larger events (M>6) where finite-source dimensions are not yet constrained. The addition of ground motion observations (or observed macroseismic intensities) reduces uncertainties over data-constrained portions of the map. Higher grades ("A" and "B") correspond to ShakeMaps with constrained fault dimensions and numerous stations, depending on the density of station/data coverage. Due to these dependencies, the letter grade can change with subsequent ShakeMap revisions if more data are added or when finite-faulting dimensions are added. We emphasize that the greatest uncertainties are associated with unconstrained source dimensions for large earthquakes where the distance term in the GMPE is most uncertain; this uncertainty thus scales with magnitude (and consequently rupture dimension). Since this distance uncertainty produces potentially large uncertainties in ShakeMap ground-motion estimates, this factor dominates over compensating constraints for all but the most dense station distributions.

Introduction

ShakeMap, a software package that portrays the extent of potentially damaging shaking following an earthquake, was primarily developed to display, and render more useful, densely recorded ground motion recordings for California. Built into ShakeMap are predictive tools meant for estimating ground motions in areas of sparse station coverage as well as interpolating between recorded and estimated peak motions. ShakeMap is produced domestically and internationally, and ranges from rather dense station coverage (California) to non-existent, particularly in real time (much of the globe). Any particular ShakeMap can be controlled by either observations or predictions, and in fact any one map is likely to have areas over which one or the other prevails.

ShakeMaps used for post-earthquake response and loss assessment are constrained in part by rapidly gathered ground motions and by intensity data via the Internet coupled with rupture dimensions resolved with rapid finite-fault analyses. Systematic estimation of site amplification on a regional or global basis, the inclusion of sparse strong-motion data and macroseismic intensities, incorporating modeled or observed rupture dimensions, and empirically predicting regionally-specific ground-motion amplitudes all provide different constraints, and contribute in unique ways to the uncertainties.

True ground motions for moderate to large earthquakes are highly variable spatially. In ShakeMap, this spatial complexity is variably sampled, leading to a rather complicated, sometimes unintuitive, pattern of shaking uncertainties. Ways to address this challenge by quantifying and then qualifying uncertainty for ShakeMap shaking patterns will be discussed later.

The short description of uncertainty is that shaking is well-constrained near seismic recording stations, and is poorly constrained away from stations where ground motion predictions must be relied on. Hence, a quick glance at any ShakeMap (for example, for the Northridge earthquake shown in Figure 1) allows a quick assessment of where the map is well constrained and where it is not. However, the actual uncertainties are more complicated and a subset of these complexities, particularly those that dominate the uncertainty will be discussed later.

Since uncertainties for the shaking-hazard estimates contribute to subsequent uncertainties in loss estimates, we first discuss our approach to quantify the ShakeMap uncertainty as a function of spatial location on the map grid. The uncertainty values computed consist of latitude/longitude grid-based multiplicative factors to be scaled by the standard deviation of the ground motion prediction equation (GMPE) used for that earthquake.

Several manual and automated systems now use ShakeMap peak-parametric values (peak acceleration, velocity and spectral accelerations) for loss estimation, including the Federal Emergency Management Agencies' (National Institute of Building Sciences and Federal Emergency Management Agency, 2003) widely deployed Hazards U.S. (HAZUS) methodology software. The HAZUS methodology is also used directly in the ShakeCast system (Porter, 2008; Wald and others, 2008). At this time, these systems do not take advantage of the knowledge of the spatial uncertainties now quantified via ShakeMap. However, Luco & Karaka (2007) indicate ways to take into account the ShakeMap spatially-varying uncertainties directly into loss uncertainty by combining building-fragility curves with ShakeMaps of the mean ground-motion estimates as well as their uncertainties. They provide an example of these calculations using the 1994 Northridge earthquake. The result is a map of post-earthquake damage-state probabilities for each of the generic building types and code levels. We expect other loss modelers will become rapidly more aware of and more capable of taking advantage of ShakeMap's newly-developed quantified ground-motion uncertainties.

Given a grid of uncertainty values for a given ShakeMap, we also describe a simple approach for providing a qualitative-uncertainty "grade" for each event for more general

assessment of ShakeMaps. This grading scale will allow one to quickly gauge the appropriate level of confidence when using rapidly produced ShakeMaps as part of the post-earthquake critical decision-making process as well as for qualitative assessments of archived or historical-earthquake ShakeMaps used for loss calibration or other purposes (for example, Allen and others, 2008). Finally, we provide several examples with ShakeMaps for important earthquakes to illustrate both the qualitative uncertainty assessment as well as the underlying quantitative uncertainty computations.

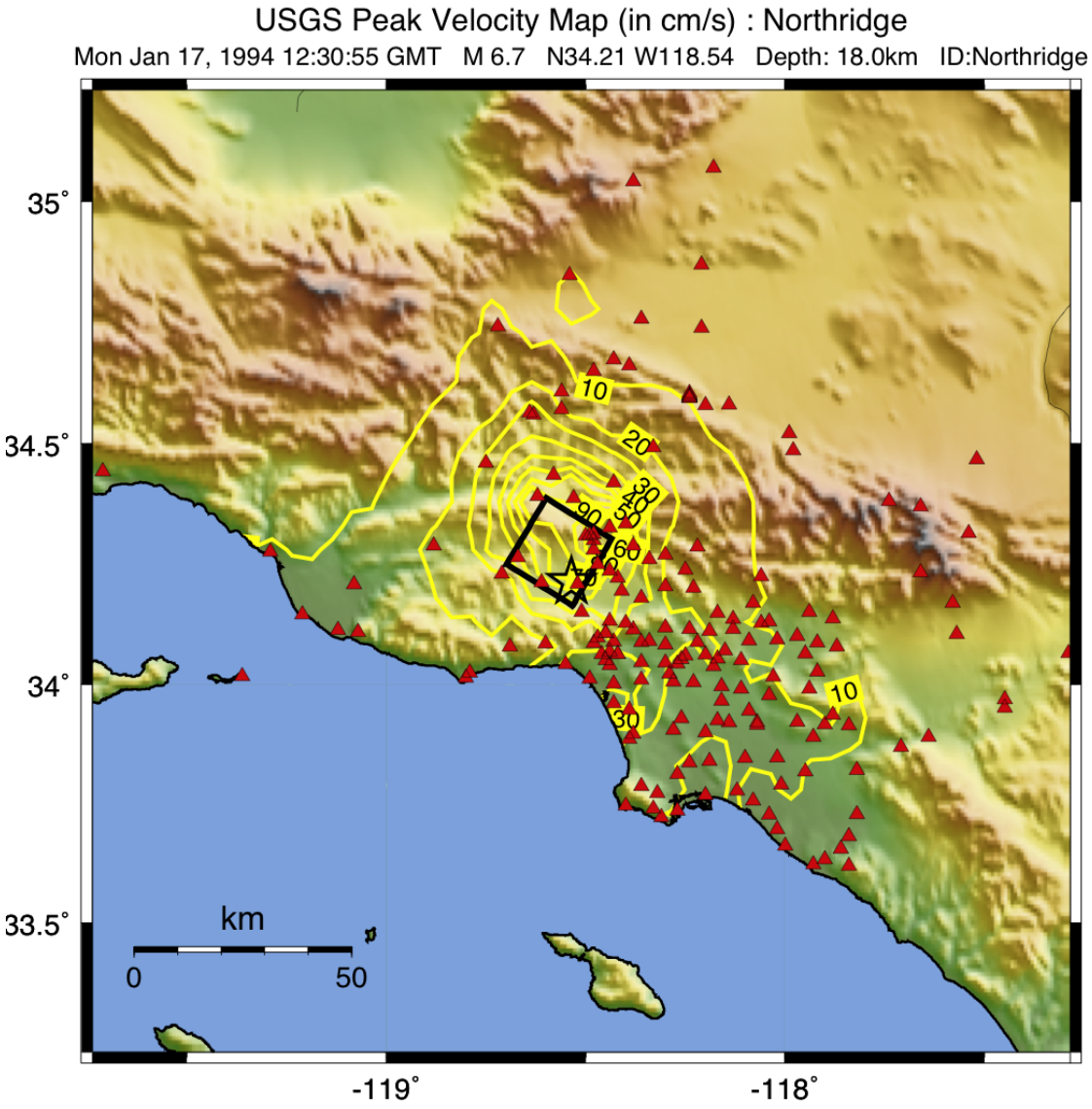

Figure 1. ShakeMap peak-velocity maps for the magnitude 6.7, 1994, Northridge, CA, earthquake. Strong motion stations are shown as triangles. The black rectangle represents the surface projection of the fault from Wald and others (1996). Contour interval is 10 cm/s.

Quantitative Shaking Uncertainty Calculations

The accuracy of a given ShakeMap varies spatially over the map area and depends on a number of contributing factors (Lin and others, 2005). However, the uncertainty is usually dominated by two aspects: (1) spatial variability of peak ground motions near intensity observations or recording stations (and hence, variability of observation density), and (2) the aleatory uncertainty associated with empirical ground-motion estimation relations used to fill in station gaps. These two sources of variability in estimating ShakeMap uncertainty are discussed; other secondary factors are also being analyzed and are therefore mentioned in passing.

Spatial variability of peak ground motions can be generalized in the form of a rapidly increasing variability with increasing distance from the nearest recording station or macroseismic observation. Aleatory variability, in contrast, is more complicated and becomes more significant as the fault dimensions get larger (about magnitude 5.5 and greater), particularly when the fault location and dimensions are not yet ascertained. Without an accurate representation of the fault-rupture geometry, the appropriate distance to a particular location—which is needed when using a forward ground-motion prediction equation—is poorly constrained. Not knowing the true distance to the fault rupture contributes significant uncertainty, particularly in the near-fault region, and this uncertainty scales with magnitude.

Our goal in quantifying ShakeMap uncertainty is to produce a grid of latitude and longitude pairs that contain not only the various peak ground-motion parameters at each point, but also contain the variance at that point for each ground-motion parameter. The average over this grid is later converted to an overall qualitative assignment of ShakeMap accuracy, as discussed in the next section. To describe the computation of ShakeMap uncertainty values at each grid point, we consider three end member cases.

Case 1) Small to moderate sized earthquake, suitable for a point source representation.

When a grid point is near a station (within 10 km), uncertainty is controlled by proximity to that station as defined by variability quantified by (Boore and others, 2003):

$$\sigma^2_{\Delta \log Y} = \sigma^2_{indobs}(1+\frac{1}{N})F(\Delta)^2 \text{ and } F = 1-e^{-\sqrt{0.6\Delta}} \quad (1)$$

where $\sigma_{\Delta \log Y}$ is the standard deviation of differences in the logarithm of the peak motion *Y*, σ^2_{indobs} is the standard deviation of an individual observation about a regression, and *N* is the number of recordings used in the average of a group of recordings in a small region. $F(\Delta)$ is a function that accounts for spatial correlation of the motion, where Δ is the distance between the sites. For this study we assumed that *N* is large enough so that the *1/N* term can be neglected. Thus, the spatial variability in ground motion reduces to zero as the distance between a grid point and the nearest station decreases to zero (fig. 2, from Boore and others, 2003). With a large grid-point-to-station distance, the spatial variability in ground motion approaches the standard deviation of the GMPE. The cut-off distance for computing spatial variability in ground motion is set at 10 km in our study.

For distances greater than 10 km, the total aleatory uncertainty (sigma) of (Boore and others, 1997) ground-motion prediction equations is used:

$$\sigma\_\text{aleatory} = \sqrt{\sigma^2\_\text{interevent} + \sigma^2\_\text{intraevent}} \quad (2)$$

With several ShakeMap data points (seismic station amplitudes), a bias term between the forward ground-motion predictions and the data can be removed, thereby effectively removing the inter-event term. However, when no data are available, no event-specific bias correction can be made and both the intra- and inter-event terms contribute (Equation 2). Note that under these conditions, the uncertainty can range from 0.0 to 1.0 times σ. (For extended sources, ground motion uncertainties are possible with multiplicative factors as large as several times σ.)

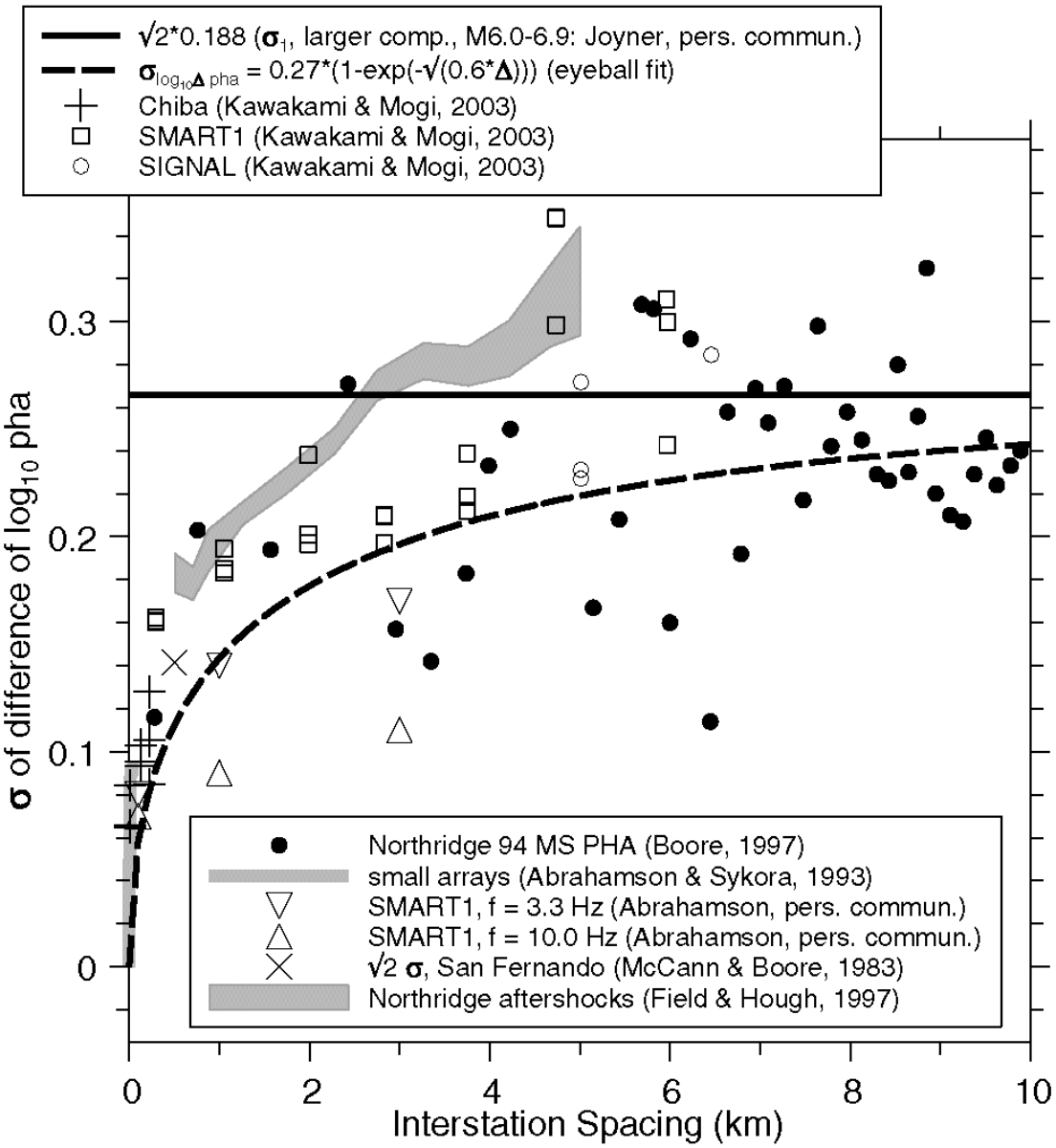

Figure 2. Standard deviation of difference of the largest peak horizontal acceleration as a function of inter-station spacing. F(Δ) given in equation 1 is shown by the curve. Data include Northridge earthquake strong motions (Boore, 1997) and previous studies as indicated (figure from Boore and others, 2003).

Case 2) Large earthquake, where fault rupture geometry and dimensions are not known.

For earthquakes of magnitude 5.5 and larger, the fault dimension affects one's measure of the distance from the fault to the site of interest. When employing the Joyner-Boore distance measure used for forward ground-motion estimation, the fault-rupture dimension must be known. Recall that the Joyner-Boore distance is defined as the closest distance from a site to the surface projection of the fault rupture. If necessary, initial ShakeMaps are produced without knowledge of the rupture dimensions. Again, the uncertainty is generally low near the seismic stations, but at some distance from the stations it is constrained only by the forward predictions using a GMPE and knowledge of the site condition. In this case, distance adjustments are made to convert the point-source (epicentral) distance used to the appropriate Joyner-Boore distance for the GMPE used. The aleatory uncertainty must also then be adjusted. The results and the approach defined in (EPRI, 2003), in which the distance adjustment is determined for the case where the rupture orientation is assumed to be uniformly distributed in azimuth from 0 to 360 degrees and for a mixture of strike-slip and reverse ruptures using random epicenters is adopted. Note that Scherbaum and others (2004a) regressed simulated ground motions to provide an analogous approach to source-to-site distance correction, allowing conversion from most distance measure to Joyne-Boore distances. However, the conversion provided by EPRI (2003) where previously adopted here.

For simulated ruptures, (EPRI, 2003):

- Computed the appropriate distance measure and corresponding median ground-motion parameter,
- Considered the geometric mean of all these simulation values to be the median ground motion for that epicentral distance and magnitude,
- Inverted the median ground motion to find the distance that corresponds to that median ground motion value,
- Determined a distance-adjustment factor for each epicentral distance, magnitude, and ground motion parameter, and
- Fit these distance-adjustment factors with a functional form, and provided the necessary coefficients in a series of look up tables.

Using the distance-correction factor then simply entails employing these distance-adjustment relationships (EPRI, 2003) that translate epicentral to the equivalent Joyner-Boore distance:

$$r_{Joyner-Boore} = r_{Epicentral} \times \{1 - 1/\cosh(C_1 + C_2(M-6) + C_3 \ln(r'))\} \quad (3),$$

$$\text{where } r' = \sqrt{r_{Epicentral}^2 + h^2} \quad (4), \quad \text{and} \quad h = e^{C_4 + C_5(M-6)} \quad (5),$$

$r_{Joyner-Boore}$ is the Joyner-Boore distance, $r_{Epicentral}$ is the epicentral distance, M is the magnitude of the earthquake, and $C1$ to $C5$ are the (EPRI, 2003) model coefficients (which vary by ground-motion model and seismic frequency) given in Table 1.

Table 1. Distance adjustment from epicentral to Joyner-Boore distance coefficients for equations 3 and 5 (random epicenters) [from Table 3-38 of (EPRI 2003)]

Frequency(Hz)	C1	C2	C3	C4	C5
0.5	-0.4098	-1.394	1.003	1.235	1.421
1.0	-0.4060	-1.394	1.003	1.237	1.424
2.5	-0.4066	-1.394	1.003	1.235	1.426
PGA	-0.4517	-1.394	1.003	1.239	1.431

For large events, using the epicentral distance would underestimate ground motions near a finite fault (since it is the maximum possible source-station distance). Hence, when the fault geometry and orientation is not known, we have adopted these distance adjusted ground motions for ShakeMap production and a mean value of ground motion at each point is provided rather than the simple epicentral distance-based estimation. As described above, the mean value is based on random-fault geometry and epicenter. (If and when faulting geometry is established, actual Joyner-Boore distances are computed from the fault location (see Case 3).)

The variability associated with this distance adjustment is also derived in EPRI (2003). The variability in the median ground motion, due to the randomness in epicenter location and rupture orientation, was used to compute a ground motion standard deviation and we employ their equations to compute the additional component of aleatory uncertainty:

$$\sigma\_addptsr = e^{C1+C2(M-6)+C3(M-6)^2} \times [1 - 1/\cosh(f_a)] \times 1/\cosh(f_b) \qquad (6),$$

$$f_a = e^{C4+C5(M-6)} + e^{C6+C7(M-6)} \times r_{Epicentral} \qquad (7),$$

$$f_b = e^{C8+C9(M-6)} \times \ln(r'/h), \qquad (8),$$

$$r' = \sqrt{r_{Epicentral}^2 + h^2}\ ,\ h = e^{C10+C11(M-6)} \qquad (9),$$

where $\sigma\_addptsr$ is the point source aleatory, $r_{Epicentral}$ is the epicentral distance, M is the magnitude of the earthquake, and C1 to C11 are the model coefficients given in Table 2 (from EPRI, 2003). We can then combine this additional point source variability (Equation 7) with that associated with the prediction equation (Equation 2):

$$\sigma\_\text{total} = \sqrt{\sigma^2\_\text{aleatory} + \sigma^2\_\text{addptsr}} \qquad (10)$$

Table 2. Additional aleatory variability (random epicenters) coefficients for equations 6–9 [from Table 3–42 of (EPRI 2003)]

Frequency(Hz)	C1	C2	C3	C4	C5	C6	C7	C8	C9	C10	C11
0.5	-1.502	0.5506	-0.03874	-0.8330	-0.01935	-1.341	-0.6375	-0.1008	0.3328	1.564	1.635
1.0	-1.604	0.6415	-0.05674	-0.8626	-0.01209	-1.177	-0.7274	-0.1472	0.4290	1.722	1.635
2.5	-1.430	0.5386	-0.03777	-0.7968	-0.04394	-1.378	-0.6413	-0.1241	0.3472	1.607	1.630
PGA	-1.407	0.5926	-0.05345	-0.8708	-0.001605	-1.305	-0.7161	-0.1846	0.3675	1.599	1.629

In case 2, the multiplicative factor for σ (not considering stations for the moment) can be greater than 1.0, and approaches approximately 3.0 for magnitude 8 earthquakes.

Case 3) Large earthquake, where fault rupture geometry and dimensions are known.

Here, the uncertainty is greatly reduced in comparison to the point-source approximation as the site-to-source distance can be calculated accurately. In case 3, the multiplicative factor for σ cannot be greater than 1.0, and as in case 1, it is lower near stations.

The calculations described above provide a single uncertainty value at each grid point used to compute the ShakeMap (see Wald and others, 2005, for more details on ShakeMap interpolation). At this time these values are not frequency- or ShakeMap metric-dependent, as discussed later. From a bookkeeping perspective, these values are provided in the output grid file associated with each ShakeMap (Wald and others, 2005). For each grid, the nominal value of σ for that event is given such that total uncertainty values at a given point are the product of the grid value and the GMPE σ value provided.

Qualitative Uncertainty Assignments

In addition to a spatially-dependant, quantitative assessment, many users seem to prefer a simple, qualitative grading for the entire ShakeMap. To do so, the mean uncertainty over the ShakeMap area at on-land grid cells that have intensities of VI (6.0) or greater is computed. This requirement focuses the calculation of uncertainty only on portions of the map with potentially damaging ground motions. In contrast, inclusion of lower intensities would make the average uncertainty map-scale dependent. Under such circumstances, simply resizing the map could result in a different uncertainly grade, a condition that should be avoided.

For all on-shore grids points, for which the computed intensity is greater than VI, the average uncertainty factor, $\bar{\sigma}$, is computed by summing grid-cell uncertainties and dividing by the total number of cells meeting these criteria. For each cell, the scale factor is the value determined for adjusting the GMPE σ value based on the appropriate case outlined above.

After computing the mean uncertainty value for the region of intensity VI or higher, letter grading "A" through "F", for high to poor quality, respectively, are assigned based on a subjective assignment of the average values to grades. Our goal was to have the middle-range ("C") grade correspond to a ShakeMap for a moderate-magnitude earthquake suitably represented with a point source location. Thus, we assign a value of $\overline{\sigma}$ of 1.0 (that is, 1.0 times the aleatory uncertainty for the GMPE used) to the letter grade of “C” which refers to an “average” performance.

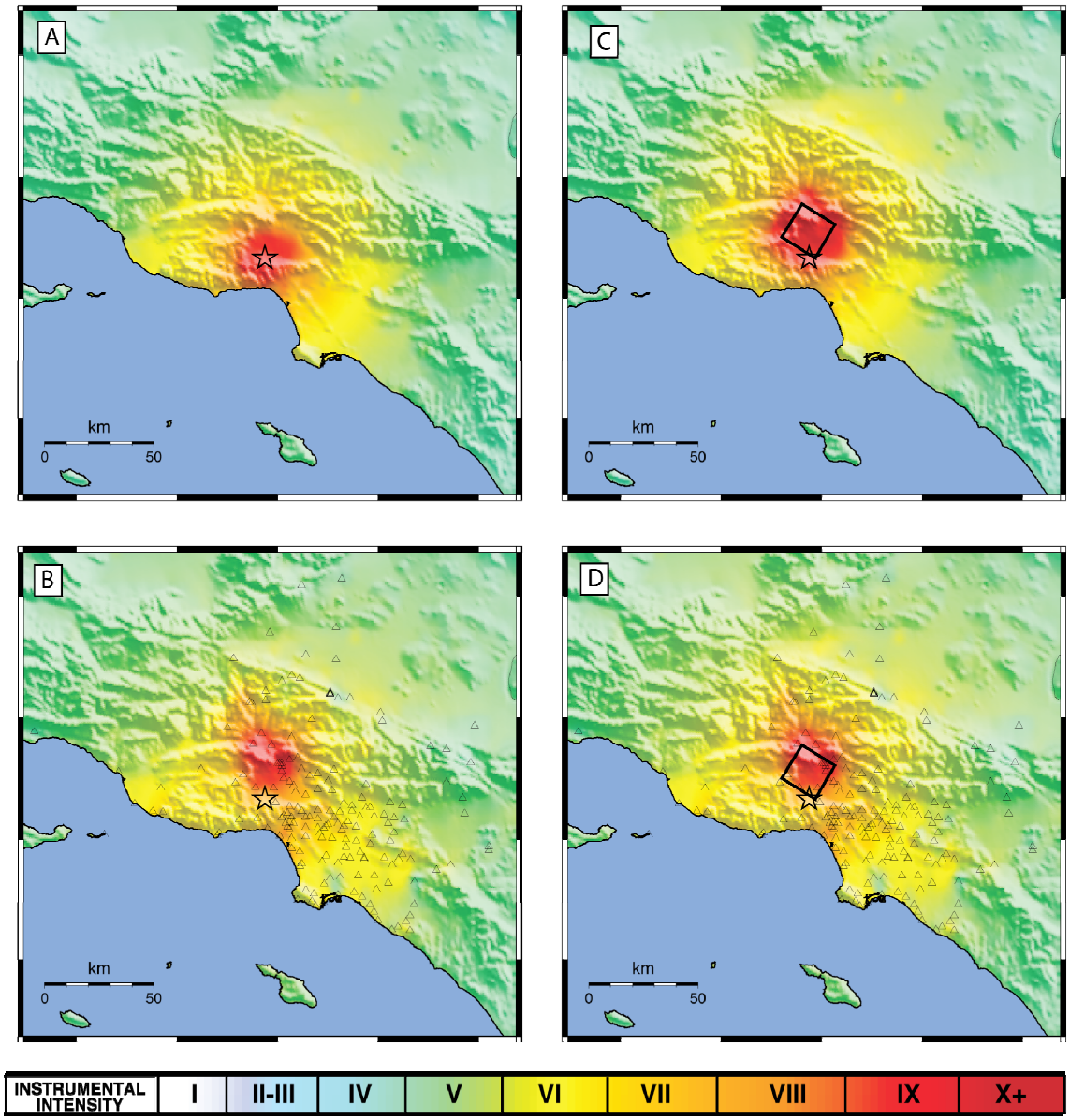

Figure 3. ShakeMap Instrumental Intensity maps for the 1994 Northridge, CA, earthquake. A) Constrained only by magnitude (M6.7) and epicenter, using median distance estimates (see text for details); B) Constrained by magnitude, epicenter, strong motion stations (triangles), and inter-event bias term (see text); C) Constrained by magnitude, and fault dimensions (black rectangle represents the surface projection of the fault from Wald and others (1996); D) Constrained by magnitude, fault dimensions, stations, and inter-event bias.

For larger events (M>6) where finite source dimensions are not yet constrained, higher average uncertainty values of $\bar{\sigma} > 1.0$ indicate more poorly constrained ShakeMaps and are assigned lower grades "D" and "F". The addition of ground-motion observations (or observed macroseismic intensities) reduces the average uncertainties ($\bar{\sigma} < 1$), by reducing uncertainties over

data-constrained portions of the map. Higher grades ("A" and "B") correspond to ShakeMaps with constrained fault dimensions and numerous ground-motion observations, depending on the density of station/data coverage. Thus, the letter grade can change with subsequent ShakeMap revisions if more data are added, or when finite-faulting dimensions are established and introduced into the ShakeMap input constraints (see Wald and others, 2005).

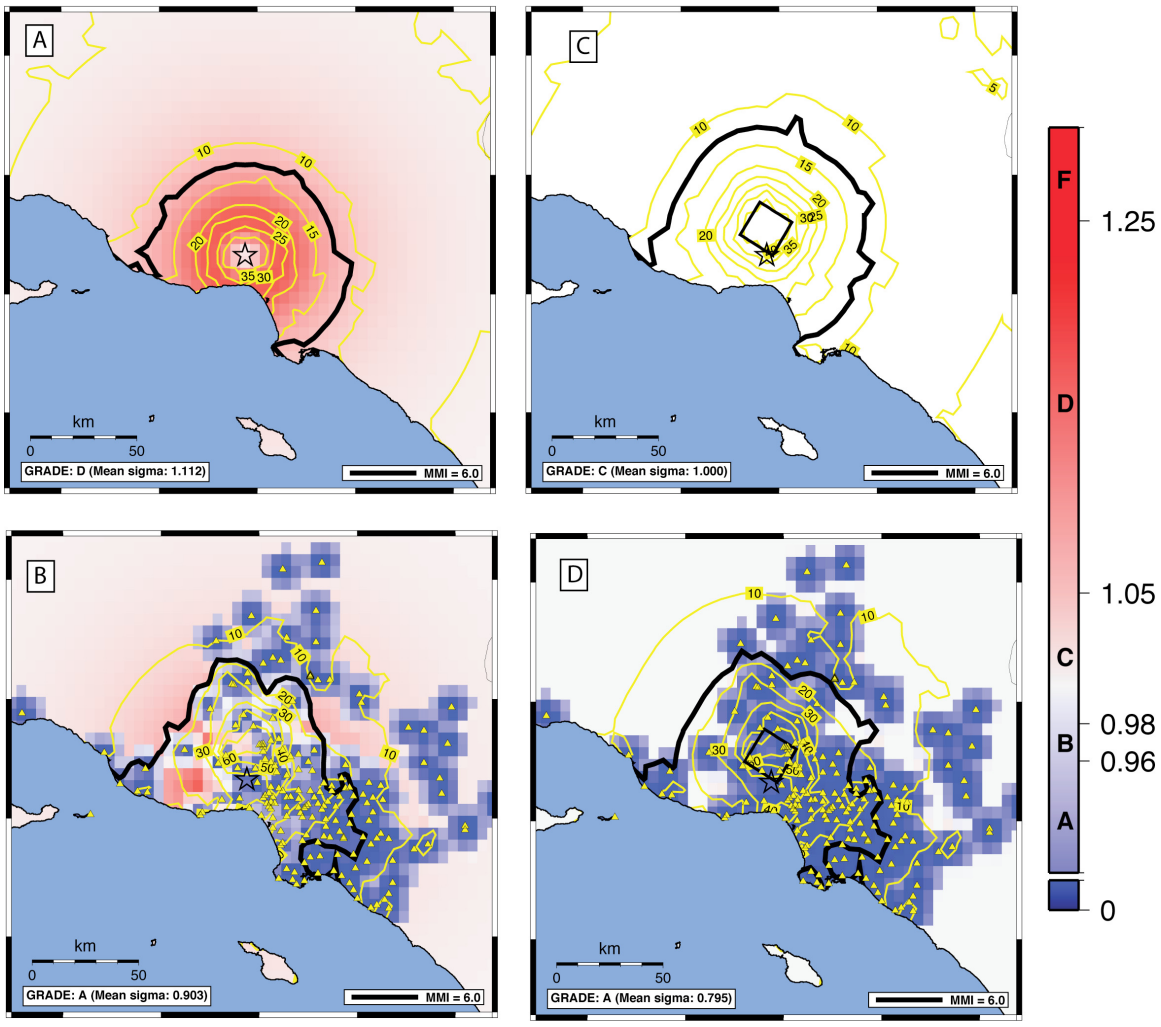

Figure 4. ShakeMap uncertainty maps for the 1994 Northridge, CA, earthquake corresponding to intensity maps in Figure 3. A) Constrained only by magnitude (M6.7) and epicenter, using median distance estimates (see text for details); B) Constrained by magnitude, epicenter, strong motion stations (triangles), and inter-event bias term (see text); C) Constrained by magnitude, and fault dimensions (black rectangle represents the surface projection of the fault from Wald and others (1996); D) Constrained by magnitude, fault dimensions, stations, and inter-event bias. Scale bar on right depicts spatial uncertainty as a linear multiplicative factor to the GMPE uncertainty; Letters refer to the corresponding letter "grade" (see text for details).

For rapid and easy assessments of the uncertainty of a ShakeMap, color-coding is introduced such that red-colored areas are poorly constrained, white-colored areas are as uncertain as the ground motion prediction equation, and blue-colored areas are better constrained (near to constraining seismic stations). Color-coding of the average uncertainty, $\bar{\sigma}$, is similarly colored, commensurate with the letter grade assigned. The scale bar shown in Figure 4 and examined more closely with Figure 5 is the qualitative-uncertainty scale bar used in subsequent uncertainty figures. Letter grades "A" thru "F" indicate high to poor quality maps, respectively delimited by ranges of the average-uncertainty label to the right. Numerical limits of 0.96, 0.98, 1.05, and 1.25 delimited subjective letter-grade cutoffs. The average value, and the corresponding letter grade on the scale to the right, is displayed on the bottom left of the uncertainty ShakeMap (see for example, Figure 4). The region of intensity VI or higher, over which the average uncertainty is computed, is show with a bold, black line (fig. 4).

For a map to be mostly red ("D" or "F" grades), fault finiteness must be substantial and the fault location unknown. White maps ("C" grades) are either small events with few data, or larger events for which the fault location and dimensions are specified. Blue maps ("A" or "B" grades) require numerous seismic stations and, for large events, specification of the fault dimensions. This grading scale allows one to quickly gauge the appropriate level of confidence when using rapidly produced ShakeMaps as part of the post-earthquake, decision-making process and for qualitative assessments of archived or historical earthquake ShakeMaps.

Another way to consider the uncertainty scale bar is in terms of absolute uncertainty of the intensity values mapped. It turns out, conveniently, the color "white" (uncertainty factor of 1.0) indicates a ± 1 intensity unit uncertainty. Since σ for peak ground velocity is approximately a factor of 2.0 (Boore and others, 1997), and instrumental intensity increases approximately one unit of intensity for a factor of two increase in velocity (Wald and others, 1999), for an uncertainty scaling factor of 1.0 the intensity uncertainty is approximately ± 1 intensity unit.

Initially, we considered other algorithms for computing the average uncertainty. For example, there are some advantages to only considering those areas of the ShakeMap that have a population actually exposed to the shaking. The rational there was that uncertainties in shaking were only relevant for areas where there are exposed assets that could experience damage, and at intensity levels at which damage could occur. That is, uncertainty in shaking values within urbanized areas should be considered. Using the LandScan2006 (Bhaduri, 2002) database, the average uncertainty scaled by the intensity level as well as the logarithm of the population at that grid cell, normalized by the grid cell area is computed:

$$U = \frac{1}{n}\sum_{i=1}^{n}\frac{(MMI(i)-6.0)\times\log(Pop(i))\times\sigma(i)}{Area(i)}$$

Subsequent testing against numerous earthquakes revealed that this approach suffered from several shortcomings. First, the lack of exposed population implies the maps have low uncertainty, whereas there may be critical facilities (for example, power plants, pipelines, or airports, etc.) where there is no permanent population in the census or LandScan data. In assessing impact, accuracy of the shaking estimates at these facilities could be an important factor to consider. Second, for a ShakeMap with a large source area away from a populated region, the calculation weighting population density would minimize the true uncertainty in ground shaking over most of the ShakeMap. Such an approach would be confusing, particularly without direct referral to a corresponding population map.

Likewise, there are two main reasons why uncertainties for small- to moderate-sized earthquakes that do not generate intensity VI are not considered. First, the lack of damage means loss calculations are not needed. Second, a lower overall range of intensities is produced (I–V) than for larger events (I–X), so the total potential range of intensities, and thus uncertainties, is rather limited.

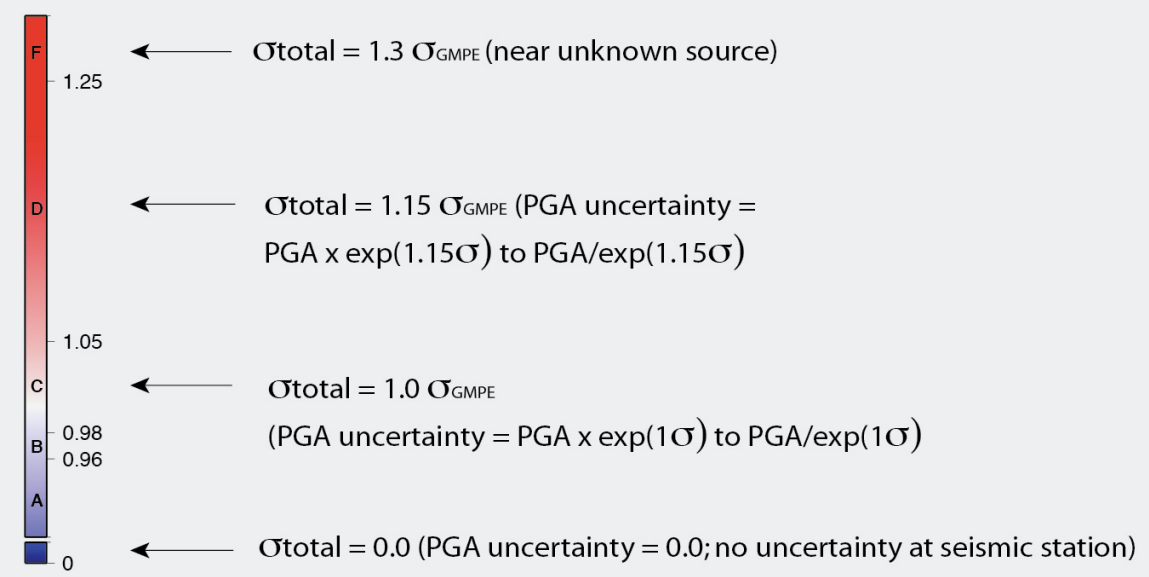

Figure 5. ShakeMap uncertainty scale bar. The decimal values at the right of the scale bar are the multiplicative factor to scale the uncertainty from the ground-motion prediction equation used. Zero uncertainty (blue) occurs at seismic stations; high uncertainty (red) occurs close to a unconstrained finite-fault source region. Letter "grades" are provided for the average uncertainty on a given ShakeMap, on land and within the zone of intensity VI or greater. See text for further details.

ShakeMap Uncertainty Examples

In this section, illustrative examples showing a wide range of the uncertainty cases are presented. For each case, the example represents actual data and constraints, with varying choices of which subsets of the data to use. In near real-time ShakeMap applications, the availability of data for different regions domestically and around the globe vary dramatically, and these examples were chosen to be illustrative the range of possible source and data constraints expected.

Northridge, California

A comprehensive example of the uncertainty calculation is presented in Figures 3 and 4 for the case of the 1994 magnitude 6.7 Northridge, California, earthquake. The maps on Figure 3 are ShakeMaps, with increasing source and data constraints (Figures 3A–D), and thus increasing overall accuracy (Figures 4A–D).

Figure 3A shows a ShakeMap based on magnitude, epicenter, and a point source rather than a finite fault representation. Thus, epicentral distance is used to compute ground motions. Figure 4A, the corresponding uncertainty map, shows a representative pattern with accuracy indicated by reddish, donut shape. Since the epicenter must be on the fault, the true distance there is known (and

is zero). Uncertainty is at its maximum at approximately one fault distance from the epicenter, because that location could be either on the fault or as far as one-fault-length away. With greater distances, the uncertainty returns to the background 1-sigma level of the prediction equation used since epicentral versus fault distance approach the same value.

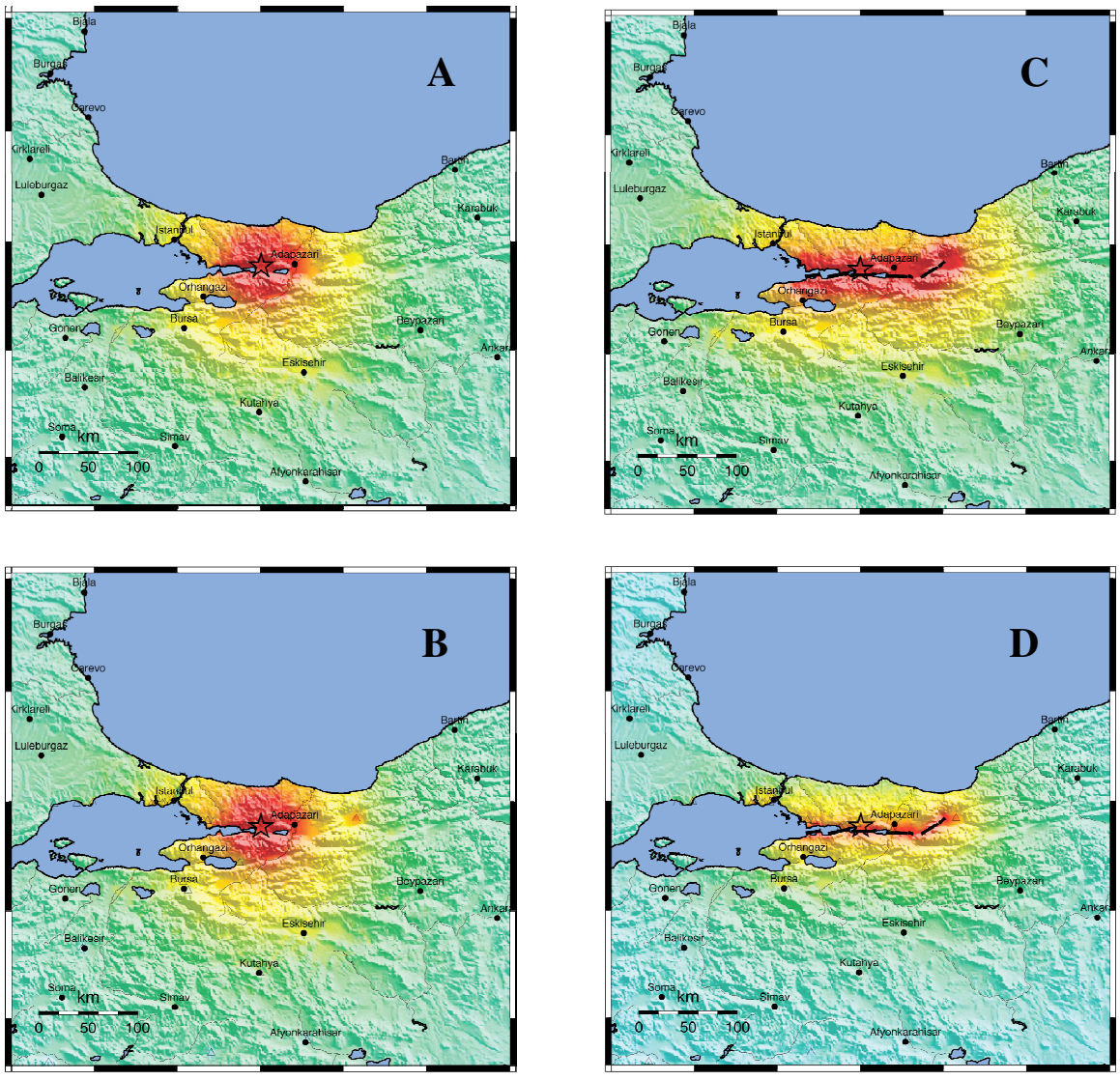

Figure 6. ShakeMap Instrumental Intensity maps for the 1999 Koeceli, Turkey, earthquake. A) Constrained only by magnitude (M7.6) and epicenter, using median distance estimates (see text for details); B) Constrained by magnitude, epicenter, strong motion stations (triangles), and inter-event bias term (see text); C) Constrained by magnitude, and fault dimensions (black line represents the fault trace); D) Constrained by magnitude, fault dimensions, stations, and inter-event bias.

Figure 3B shows a ShakeMap with the additional constraints provided by a few hundred strong-motion peak values, and thus represents a very well-constrained map, even though the

source dimensions have not been specified. The corresponding uncertainty map in Figure 4B has significant regions with blue coloring indicating proximity to the strong-motion stations, while areas with few stations are indicated by areas of red with more uncertain shaking levels. Recall, if at any time a grid point is closer to a station than 10 km, the variability associated with that grid to station distance (Equation 1) controls the uncertainty and is thus lower. Since the average uncertainty-scaling factor is less that 0.96, this ShakeMap receives a letter grade of "A" (fig. 4B).

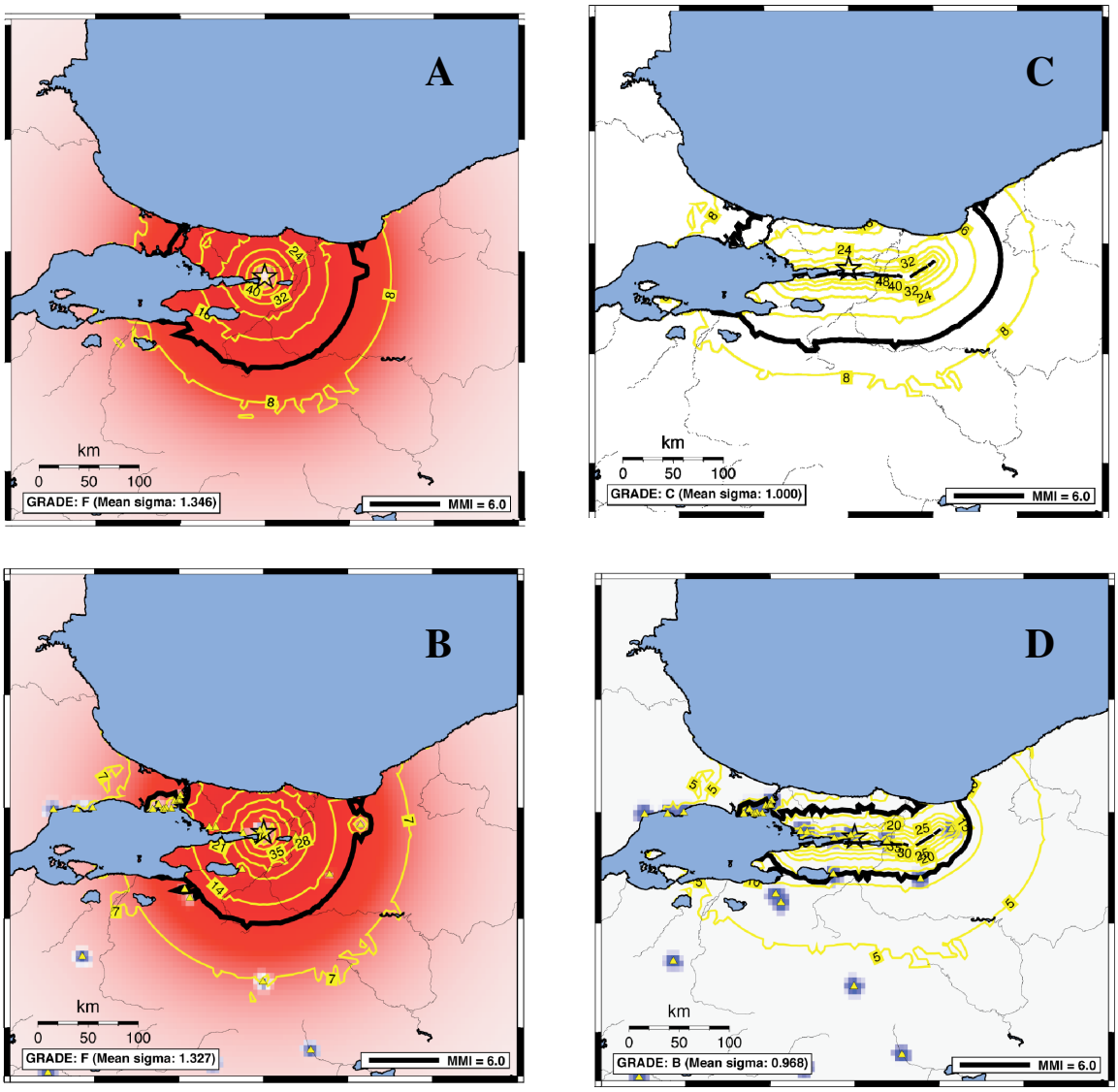

Figure 7. ShakeMap uncertainty maps for the, 1999 Koeceli, Turkey, earthquake corresponding to intensity maps in Figure 6. A) Constrained only by magnitude (M6.7) and epicenter, using median distance estimates (see text for details); B) Constrained by magnitude, epicenter, strong-motion stations (triangles), and inter-event bias term (see text); C) Constrained by magnitude, and fault dimensions (black line represents the fault trace); D) Constrained by magnitude, fault dimensions, stations, and inter-event bias. The uncertainty color scale and corresponding letter "grades" are shown in Figure 4.

For the ShakeMap in Figure 3C, fault finiteness is added, improving the distance measure to be $r_{Joyner-Boore}$, but for this example, the strong-motion stations have been removed. Adding the fault dimension alone is equivalent to Case 3 described above, so the uncertainty is uniform (Fig. 4D), with a ratio equal to 1.0 times sigma, since fault distances are known at all points on the map. The ShakeMap is effectively the direct application of the GMPE, unimproved by any ground-motion recordings; this is the equivalent of an earthquake scenario, where source is specified but no data exist.

Finally, for a well constrained ShakeMap, with both abundant strong-motion data and specified fault dimensions (Figure 3D), uncertainty in all areas is equal to or less than 1.0 times sigma. In Figure 4D, the corresponding uncertainty map, blue indicates location of strong motion stations where no there is no uncertainty in the shaking level since the value is recorded there. All other portions of the map are white, indicating 1-sigma uncertainty values given the known fault location.

For the Northridge earthquake the source dimension was limited (roughly 20 km in length and 20 km in width), so the distance correction term (Equation 3) and the corresponding $\sigma\_addptsrc$ are relatively small additional uncertainty. Thus, even in the case shown in Figure 3A, with simple point source representation, the corresponding letter grade is “D” not “F” (Figure 4A). Larger magnitude earthquakes, with larger fault dimensions, can indicate larger uncertainties, as is the case in the next example.

Izmit, Turkey

Figures 6 and 7 show analogous ShakeMaps and corresponding uncertainty maps for the 1999 Izmit, Turkey, (M7.6) earthquake, which resulted in over 17,000 fatalities. In this case, the actual strike-slip fault dimension was approximately 120 km, so that lack of knowledge of the fault dimension greatly reduces the ability to predict ground motions employing an empirical GMPE. In addition, strong-motion station coverage in Turkey is less dense than for California, so that within the scale of the ShakeMap, only a dozen or so stations were available for this earthquake.

Since the fault is so large, the lack of knowledge of its location results in a prominent, red donut-shaped uncertainty ring (fig. 7A). The amplitude of the uncertainty scale factor is larger than for Northridge since the rupture dimension is roughly 5 times larger. Note that not only are peak uncertainty values larger, but large uncertainty values also extend over a region that scales in radius with the fault dimension (roughly 120 km).

Interestingly, for large earthquakes, if the fault dimension is constrained, the uncertainty is significantly reduced, indicating the importance of rapid determination of the fault finiteness in an earthquake response situation (fig. 7C). In contrast, and perhaps counter-intuitively, adding only a dozen strong-motion stations only slightly reduces the overall uncertainty (figs. 7B and 7C). In the ShakeMap processing, strong-motion stations only influence a limited areal extent around the station. While, overall, their presence allows removal of the inter-event variability via the bias calculation, the overall uncertainty is much more sensitive to that introduced due to the lack of knowledge of such a large fault extent.

ShakeOut Scenario, Southern California

Scenario ShakeMaps produced for the November 2008 “ShakeOut” planning exercise for southern California (Jones and others, 2007) provide another important example of the evolution of the ShakeMap uncertainty in California under circumstances for which the actual shaking values

are fully "known". That is, unlike a real earthquake, the shaking input is fully specified (fig. 8A), and the ShakeMaps presented demonstrate the actual solution with varying and increasing degrees of data and constraints (8B–D).

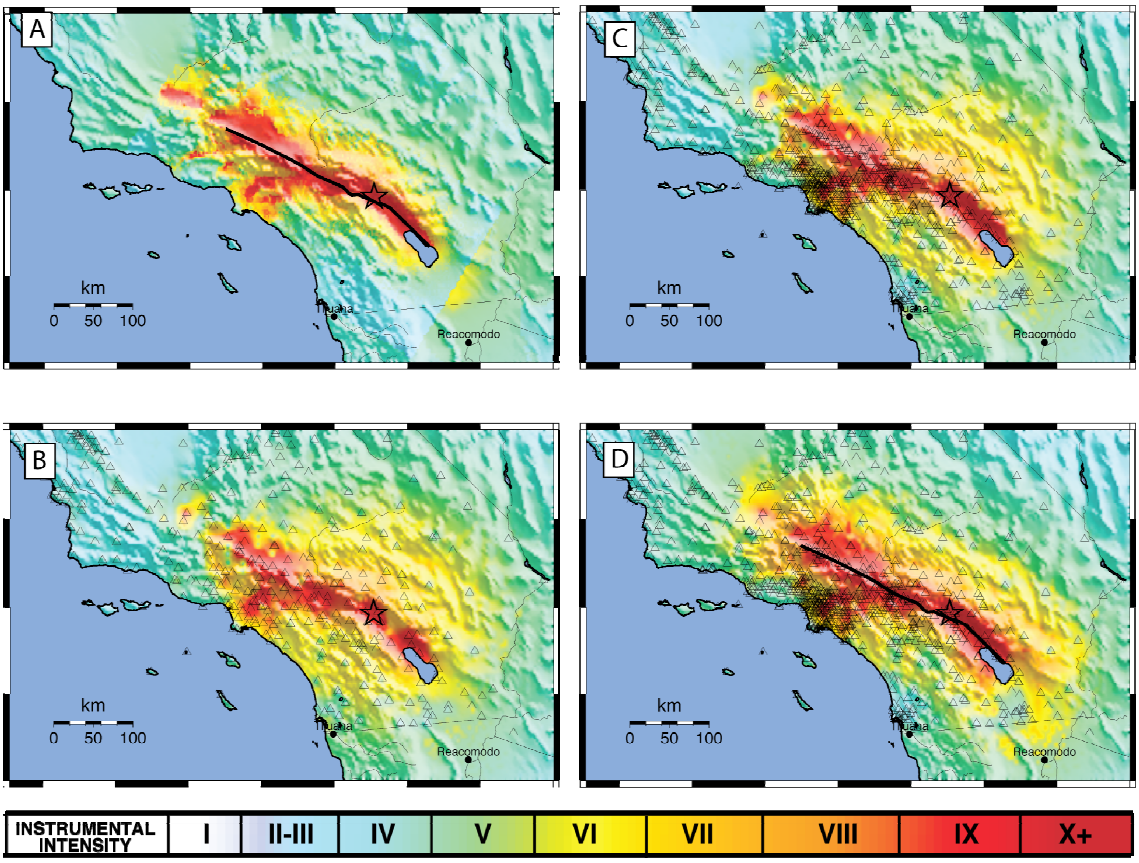

Figure 8. ShakeMap Instrumental Intensity maps for a scenario earthquake on the southern San Andreas fault, a M7.8 "ShakeOut" event developed for a November 2008 exercise in California (Jones and others, 2007). A) Predicted intensities using 3-D broadband simulations (Graves, written communication, 2008); B) Constrained by magnitude (M7.8), epicenter, and ½ of existing near real-time seismic stations; C) Constrained by magnitude (M7.8), epicenter, and all near-real time seismic stations; D) Constrained by magnitude (M7.8), fault location (black line), all near-real time seismic stations, and inter-event bias.

Figure 8A indicates the complete, simulated intensity distribution model with 3D wave-propagation computations by Graves (written communication, 2008). In figure 8B, what would be expected for a ShakeMap within about 5–6 minutes of such an event is simulated, with knowledge of the magnitude and epicenter and by randomly choosing half of the real-time strong-motion stations in the region available to ShakeMap. This value was chosen simply to simulate what may be available to ShakeMap given such a large event (some stations may still be triggered, and some may have trouble communicating immediately). With half the stations, there is a reasonable approximation (fig. 8B) to the actual intensity distribution (fig. 8A). The corresponding uncertainty map, shown in figure 9B, still shows considerable uncertainty since the area without stations is still substantially larger than areas immediately adjacent to recording stations. In fact, the overall

shaking level in areas not constrained by data is somewhat larger than the actual values; the large uncertainty (red coloring) and overall poor grade reasonably reflects this uncertainty.

Addition of the remaining strong-motion stations allows further recovery of strong shaking along the San Andreas fault (fig. 8C) but only marginally reduces the uncertainty away from these sites. Not until the fault dimension is added does the uncertainty come down on average (figs. 8D and 9D). At this point, the letter grading becomes an "A" since the distance from the fault is now constrained. Note that even in this situation (fig. 8D), the overall shaking intensity is different (higher) than "observed" (fig. 8A). This is due to the fact the 3D simulations produce ground motions that attenuate with distance with different behavior than the assumed GMPE used in ShakeMap.

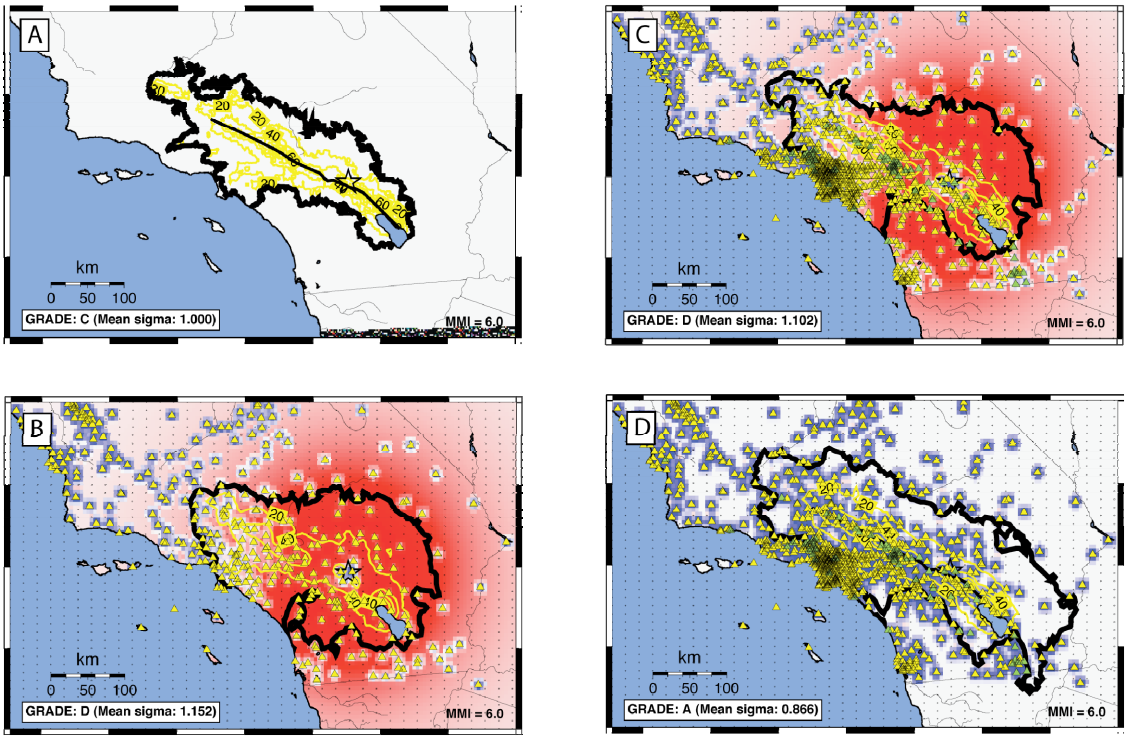

Figure 9. ShakeMap uncertainty maps corresponding to southern San Andreas Fault, M7.8 "ShakeOut" scenario maps shown in figure 8. A) Predicted intensities using 3-D broadband simulations (Graves, 2007); B) Constrained by magnitude (M7.8), epicenter, and ½ of existing near-real time seismic stations; C) Constrained by magnitude (M7.8), epicenter, and all near-real time seismic stations; D) Constrained by magnitude (M7.8), fault location (black line), all near-real time seismic stations, and inter-event bias. The uncertainty color scale and corresponding letter "grades" are shown in Figure 4.

ShakeMap Atlas

As part of the USGS Prompt Assessment of Global Earthquakes for Response (PAGER) Project (Wald and others, 2006), we have developed an Atlas of ShakeMaps for historical earthquakes. The Atlas has emphasis on events that have caused casualties and those for which secondary constraints (Macroseismic, strong motion, faulting) are available in the literature or via databases (Allen and others, 2008).

As an example of the procedure for generating Atlas ShakeMap, the 1994 Northridge, California earthquake is revisited, but this time with only macroseismic data. The macroseismic data (Modified Mercalli Intensity, MMI) are from the USGS "Did You Feel It?" system (Wald and others, 1999a). Figure 10A shows the Northridge earthquake ShakeMap resulting from several hundred intensity observations, and the resulting uncertainty map (fig. 10B). The dense MMI observations provide shaking constraints over almost the entire near-source region, resulting in a very low uncertainty grade, even without constraint from the fault location. Note that the addition of "Did You Feel It?" data is particularly useful in some instances to reduce uncertainty for a ShakeMap. In particular, in many areas of the United States, where few stations are available but for which population is relatively dense, fairly low-uncertainty intensity maps can rendered rather quickly (tens of minutes) after the event with the addition of these data.

That the observations in this case are MMI, not strong-motion recordings, means there would be additional uncertainty associated with the conversion to peak acceleration and velocity (Wald and others, 1999b). However, the main use of the ShakeMap Atlas events is to derive loss functions based on MMI from historic earthquakes and their associated fatalities. In that sense, the fact that the ShakeMaps are constrained by MMI observations does not add additional uncertainty to the intensity map, only to the peak-acceleration, peak-velocity, and spectral-acceleration versions of the ShakeMaps. Naturally, intensity assignments themselves are somewhat subjective and entail their own uncertainties.

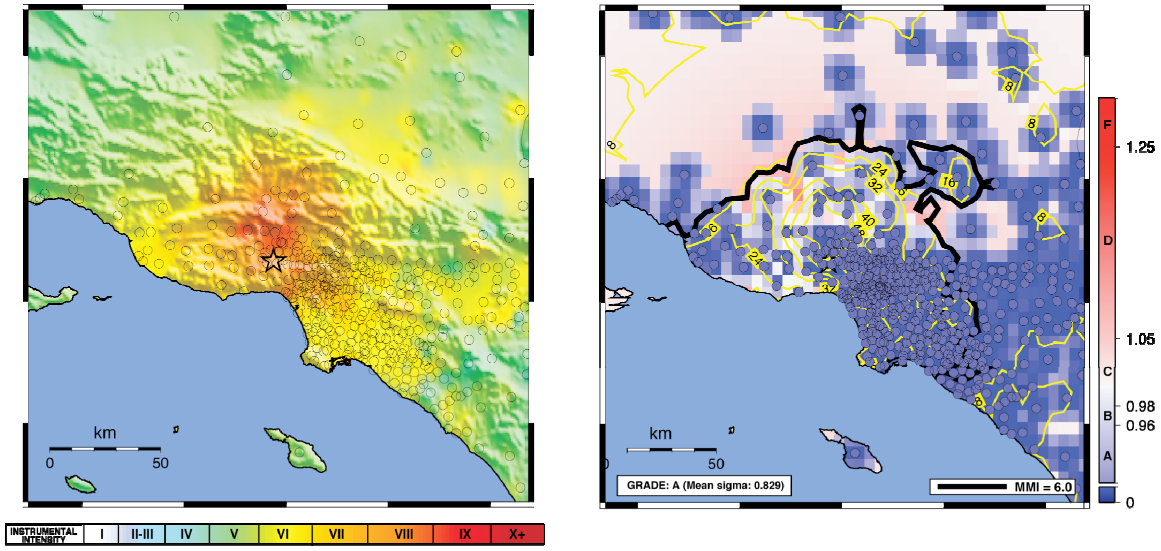

Figure 10. ShakeMap Instrumental Intensity map (left) and corresponding uncertainty map (right) for the 1994 Northridge, CA, earthquake. The ShakeMap is constrained by the magnitude (M6.7), epicenter, intensity observations ("Did You Feel It?" circles) and inter-event bias term (see text). Compare the intensity distribution and uncertainty maps with those constrained by strong-motion observations shown in figures 3B and 4B, respectively.

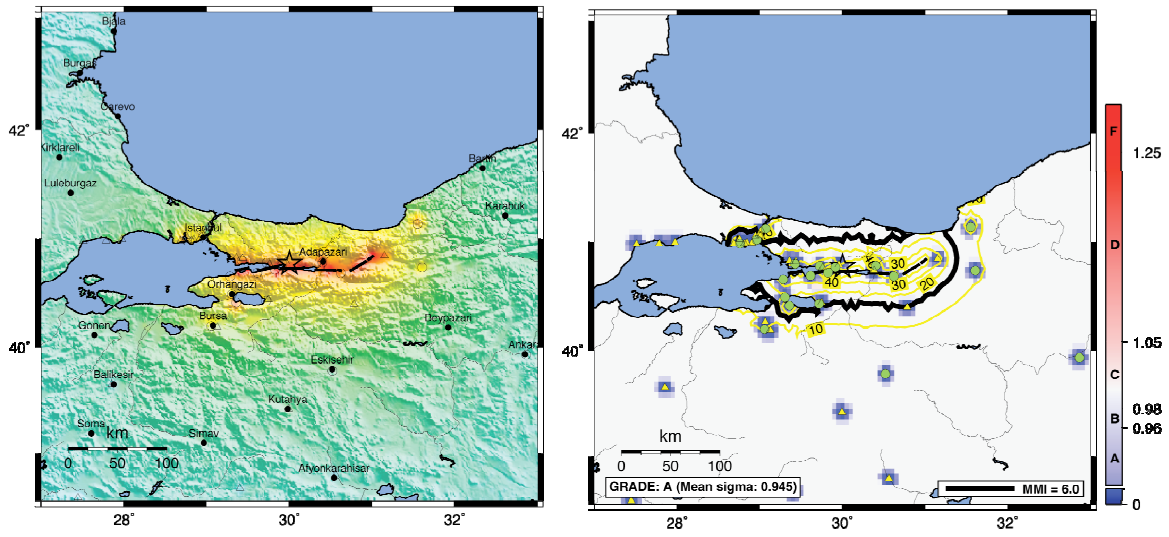

Figure 11. ShakeMap Instrumental Intensity map (left) and corresponding uncertainty map (right) for the 1999 Koeceli, Turkey, earthquake. The ShakeMap is constrained by the magnitude (M7.6), epicenter, intensity observations (circles) and inter-event bias term (see text). Compare intensity distribution and uncertainty maps with that constrained by strong-motion observations shown in figures 6D and 7D, respectively.

A second example of the uncertainties for the ShakeMap Atlas is for the 1999 Izmit, Turkey, earthquake. In figure 11, we have now added dozens of MMI observations. Augmenting the fault location and few strong motion stations with the MMI data results in a reasonably well-constrained map (fig 11, right). For the purposes of loss calibration, the letter grading for such events can be used for relative weighting of historic events. For a collection of historic earthquakes ShakeMaps, higher quality ShakeMap can be given greater weighting than more poorly constrained events, the latter typically being relatively large events without as much MMI data and/or lacking fault constraints.

Discussion

While we attempt to model the dominant sources of ShakeMap uncertainty, many other factors also contribute that are not explicitly addressed at this time. For example, with the Global ShakeMap System, in many cases we rely on hypocentral locations that are constrained from teleseismic data alone, with few regional or nearby seismic stations. We have yet to quantify the contribution to shaking uncertainty due to potential hypocentral-location error (latitude, longitude, and depth), both for the point-source approximation and as it pertains to the relative location of a finite-fault model. For a regional network with small location errors, this contribution to uncertainty can be ignored, but for teleseismic-source locations, errors can be on the order of 10 km. A brute force approach would be to iterate over a range of potential hypocentral locations consistent with the location uncertainty bounds, but one must iterate both horizontally as well as with depth.

Rapidly-determined magnitudes also are uncertain, but an overall scaling for amplitude biases can be, in part, accommodated by the ShakeMap bias correction (Wald and others, 2005). Hence at this time we do not explicitly account for magnitude uncertainty for rapidly determined

ShakeMaps. For Scenario or Altas ShakeMaps, magnitudes are assumed to be either assigned or relatively well constrained.

As far as accuracy of the chosen fault dimensions are concerned, we assume that they are approximately as well known as those used in the derivation of the GMPE's. Therefore uncertainty in ShakeMap fault locations is included implicitly in the GMPE uncertainties. Currently, the uncertainty calculations are limited to the Joyner-Boore distance measure; this needs to be expanded to subduction zone rupture geometry uncertainty as well. As mentioned earlier, for large earthquakes, distance-adjusted ground motions are used in ShakeMap. That is, rather than epicentral distance, the mean distance (r' in equations 3 and 4) is used, increasing the near-source shaking amplitudes in comparison to epicentral distance. For subduction geometries, where 3-D source to site measures apply in any GMPE, this correction approximately holds for shallow ruptures and does not contribute for deep events.

While it is assumed that good station coverage helps constrain a ShakeMap overall, other than the overall bias correction (which does improve the entire map quality), stations have little influence other than in their immediate vicinity. Yet, these data could be used in an automated fashion to determine source directivity (Boatwright, 2007), or source finiteness (Dreger and Kaverina, 2000), but currently these approaches are not done as rapidly as ShakeMap in California is delivered. In fact, the greatest uncertainties are associated with unconstrained source dimensions for large earthquakes where the distance term in the GMPE is most uncertain; this uncertainty scales with magnitude (and thus rupture dimension). Since this distance uncertainty can produce large uncertainties in ShakeMap ground-motion estimates, this factor dominates over compensating constraints for all but extremely dense station distributions.

Site amplification, both from our approximation of site conditions with geologically- (Wills and others, 2000) or topographically-based approaches (Wald and Allen, 2007) also add uncertainty in our shaking estimates. Likewise, potential 3-D effects can affect regions of the map in either a focused or coherent fashion, resulting in systematic over- or under-predictions of shaking. Both these effects are not explicitly addressed here. However, when recordings sample these effects (for example, a station within a basin), interpolation from those observations to nearby interpolated grid points implicitly include basin effects recorded at that station.

Future Considerations

In our analysis, we describe ShakeMap uncertainty associated with a single-parameter, peak ground acceleration. We then assume these values can be transferred directly to peak ground velocity and thus instrumental intensity via the established relations between peak ground acceleration and velocity with intensity. Intuitively, spatial variability should depend not only on distance but also on frequency, since amplitude- and frequency-dependent amplification and attenuation trade off in complex ways. However, there are few well-established studies that quantify the spatial variability of strong ground motions both as a function of distance from a recording site and as a function of frequency.

Recent analyses by Goda and Hong (2008) provide the framework for simply replacing the Boore and others (2003) peak acceleration-based function with frequency-dependent relations. Goda and Hong (2008) summarize their findings for spatial intra-event correlation versus separation distance for the parameters peak-ground acceleration (PGA) and peak spectral acceleration (PSA) as shown in figure 12 (reprinted from Goda and Hong, 2008, their figure 2). However, note that Goda and Hong (2008) have limited observations within 10 km of each other, so these regions on the curves are largely predictive. The challenge remains to better constrain

these relations at close distances. If the Goda and Hong (2008) curves could be verified for near-station distances, and as a function of peak acceleration, peak velocity, and various spectral-acceleration frequencies, we might adopt them into the general ShakeMap framework.

While the Goda and Hong PGA spatial correlation trends indicate a very similar functional form and values as Boore and others (2003), longer-period parameters indicate more spatial correlation than PGA. This makes sense as small-scale features are more likely to affect high-frequency energy. Hence, we can consider the current ShakeMap uncertainties to be conservative, likely overestimating uncertainties at longer periods, near to strong motion observations.

Using Goda and Hong (2008) relations would only affect our near-station terms, not the dominant, overall calculations for uncertainty due to unknown source dimensions. For implementation in ShakeMap, we could simply recast the uncertainty values with modified curves for distances less than 10 km from a station by replacing Equation 1 with Goda and Hong's functions, and use their coefficients for PGA and PSA (at 0.3, 1.0, and 3.0 sec) directly, and approximate peak-ground velocity (PGV) with the 1.0 PSA coefficients. Note, however, that station proximity reflects low uncertainty. Hence, improved, frequency-dependant, spatial-correlation functions will only slightly alter the uncertainty maps since overall uncertainty is dominated by regions of the map where there are few stations and which lack constraints on source rupture dimensions.

Other approaches to uncertainty calculations are possible, and further efforts are anticipated. For example, Hok and Wald (2003) addressed ShakeMap uncertainties explicitly in the context of ShakeMap calculations using a cross validation approach. By omitting individual stations from the interpolation (one at a time) and comparing estimated and recorded values (at left-out stations), they determined the uncertainty for that particular map. While this approach has the advantage of explicitly determining the uncertainty, taking into account all factors that contribute to it, it can only be determined for that particular event and station distribution. Furthermore, it can only be computed where there are actual recordings, and, more critically, it does not provide a physical description of the relative contributions of different sources of uncertainty, which could be used for subsequent ShakeMap calculations. A more physical explanation also provides incentive and the basis for which we might reduce uncertainty with more rapid recovery of fault rupture dimensions, for example.

The added uncertainty for preliminary hypocentral locations and magnitudes determined rapidly may require additional attention. Yet it is not obvious how to best address this problem. One could address it in a similar way to our approach of modifying epicentral distance to a mean distance or simply (although it would be computationally intensive) iterate on a range of locations and compute the range of motions at each site. These approaches will be explored in efforts to understand Global ShakeMap shaking, and thus PAGER loss, uncertainties.

An alternative approach for mapping of estimated ground motions and their associated uncertainties would be to regress GMPEs directly from unknown fault geometry to epicentral distance as a separate suite of relations and coefficients. This would not be a difficult task if those developing such relations were encouraged to do so routinely in the process of developing relations for fault distance. The question remains if there are enough data for large events to make this correction. In fact, Scherbaum and others (2004a) regressed simulated stochastic data to provide an analogous approach to source-to-site distance correction since presumably there were insufficient data to warrant a strictly empirical approach. The approach taken here, after EPRI (2003) produces a distance correction by iterating over all possible fault locations; in the existing data collections only a few fault geometries are sampled.

Scherbaum and others (2004b) provides a logical framework for evaluating the relative merits of GMPEs for a particular region based on observations from an independent earthquake or

several events. While there are considerable differences among published relations for any region, the use of well-established relations (like Boore and others 1997), in conjunction with the built in data-based bias correction provided in ShakeMap, reduces aleatory uncertainty in overall GMPE estimates by requiring an overall fit to the data at hand via the bias term.

Finally, Cua and Wald (2008) further explore the Bayesian approach proposed by Ebel and Wald (2003) to use both observed intensities and ground motions, along with ground motion prediction equations, to estimate peak ground motions on observed-intensity and strong-motion datasets. Cua and Wald (2008) propose a weighted-average approach for incorporating various uncertainties associated with these different types of data (observed peak ground motions, observed intensities, and predictions from ground motion prediction equations) into the ShakeMap ground-motion and intensity-estimation framework. For example, they allow assignment of the uncertainty associated with converting from observed MMI to peak ground-motion parameters and use this explicitly when combining observed (and/or converted) peak ground motions with estimated ground motions.

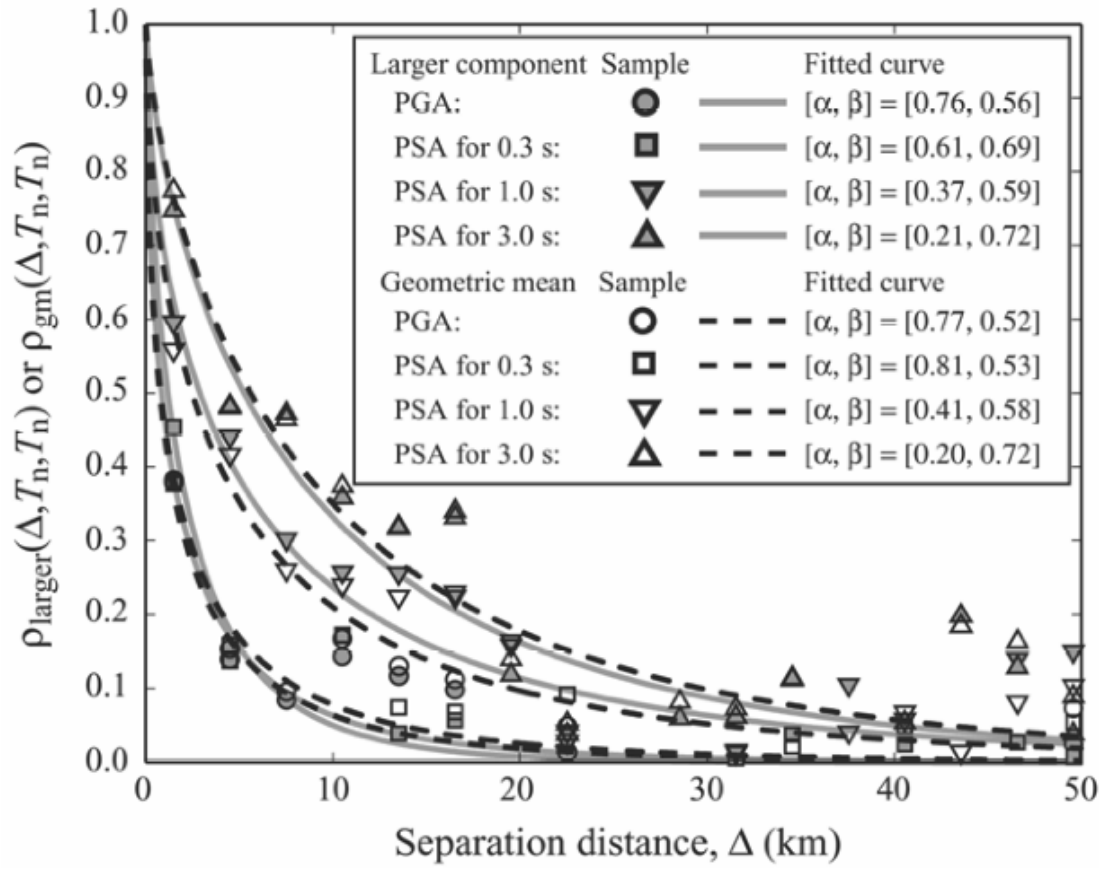

Figure 12. Estimated spatial intra-event correlation versus separation distance (Figure 2 of Goda and Hong, 2008) for PGA, PSA at 0.3, 1.0, and 3.0 sec. Goda and Hong provide separate coefficients for both the larger as well as the geometric mean of the two horizontal components.

.

Conclusions

Algorithms for quantifying and qualifying uncertainties associated with USGS ShakeMap ground motions have been developed and integrated into the suite of ShakeMap products. The uncertainty values computed consist of latitude/longitude grid-based multiplicative factors that scale the standard deviation associated with the ground-motion prediction equation (GMPE) used within the ShakeMap algorithm for estimating ground motions. The resulting grid-based "uncertainty map" is essential for probabilistic evaluation of losses derived using ShakeMaps as the hazard input.

In addition to a spatially-dependant, quantitative assessment, many users may prefer a simple, qualitative grading for the entire ShakeMap. To this end, an uncertainty letter grading ("A" through "F", for high to poor quality, respectively) based on the uncertainty map is introduced. A middle range ("C") grade corresponds to a ShakeMap for a moderate-magnitude earthquake suitably represented with a point source location. Lower grades “D” and “F” are assigned for larger events (M>6) where finite source dimensions are not yet constrained. The grading scale now implemented in ShakeMap will allow one to quickly gauge the appropriate level of confidence when using rapidly produced ShakeMaps as part of the post-earthquake critical decision-making process and for qualitative assessments of archived or historical earthquake ShakeMaps (Allen and others, 2008).

For ShakeMap, ground-motion uncertainty at any point is dominated by two main factors: (i) the influence of any proximal ground-motion observations, and (ii) the uncertainty of estimating ground motions from the GMPE, most notably elevated uncertainty due to initial, unconstrained source rupture dimensions. The uncertainty is highest for larger-magnitude earthquakes when source finiteness is not yet constrained and, hence, the site-to-source distance is also uncertain.

The addition of ground-motion observations (or observed macroseismic intensities) mitigates uncertainties, reducing uncertainties over data-constrained portions of the map. Higher grades ("A" and "B") correspond to ShakeMaps with constrained fault dimensions and numerous stations, depending on the density of station/data coverage. Thus, the letter grade can change with subsequent ShakeMap revisions if more data are added or when finite-faulting dimensions are established. The greatest uncertainties are associated with unconstrained source dimensions for large earthquakes where the distance term in the GMPE is most uncertain; this uncertainty scales with magnitude (and thus rupture dimension). Since this distance uncertainty produces such potentially large uncertainties in ShakeMap ground-motion estimates, this factor dominates over compensating constraints for all but extremely dense station distributions. Point observations only constrain nearby portions of the map.

While we have addressed the dominant sources of ShakeMap uncertainty, other uncertainties have not been addressed specifically. Additional effort could be focused on uncertainties in source location and magnitude, and geologically-based site amplification, for example. However, many of these uncertainties have been implicitly or explicitly addressed in other calculations. For example, location uncertainty, whether hypocentral or measured from a finite fault is implicit in the derivation of existing GMPEs, so as long as these same uncertainties apply in near-real time applications like ShakeMap, these uncertainties are covered.

Shaking is well constrained near seismic recording stations, and less well constrained away from such stations. A quick glance at any ShakeMap (for example, for the Northridge earthquake peak ground velocity map shown in Figure 1) allows a quick assessment of where the map is well constrained and where it is not. While we have shown that the actual uncertainties for a significant earthquake can be complicated, we must not lose sight of the fact that in areas of dense instrumentation, the maps are well constrained. Hence, a glance at the peak-xground-motion maps

(where stations are more visible than on the intensity maps) can often provide a proxy for uncertainty. However, for more sparsely instrumented regions, the new uncertainty maps themselves become an important part of the picture, particularly when making post-earthquake response decisions or for computing losses based on ShakeMap parameters.

Acknowledgments

The authors thank Anthony Shakal (California Geological Survey, CGS) for encouragement in pursuing qualitative ShakeMap uncertainty assessments and letter grading. Arthur Frankel pointed us in the direction of the EPRI report referenced heavily herein. Discussions with Bruce Worden were helpful as were reviews and comments by Trevor Allen and Bruce Worden.

References Cited

Allen, T. I., D. J. Wald, A. Hotovec, K. Lin, P. S. Earle, and K. D. Marano (2008). An Atlas of Shake-Maps for Selected Global Earthquakes, U.S. Geological Survey Open File Report, 2008–1236.

Bhaduri, B., Bright, E., Coleman, P., and Dobson, J., 2002, LandScan — locating people is what matters: Geoinformatics, v. 5, no. 2, p. 34-37.

Boatwright, J. (2007). The Persistence of Directivity in Small Earthquakes, Bull. Seism. Soc. Am. v. 97, no. 6, p. 1850–1861.

Boore, D. M., W. B. Joyner, and T. E. Fumal, 1997. Equations for Estimating Horizontal Response Spectra and Peak Acceleration from Western North American Earthquakes: A Summary of Recent Work, Seism. Res. Lett. v. 68, no. 1, p. 128–153.

Boore, D M., Gibbs, J. F., Joyner, W. B., Tinsley, J. C., and Ponti, D. J, 2003. Estimated Ground Motion From the 1994 Northridge, California, Earthquake at the Site of the Interstate 10 and La Cienega Boulevard Bridge Collapse, West Los Angeles, California, Bull. Seism. Soc. Am. v. 93, no. 6, p. 2737–2751.

Cua, G. And D. J. Wald (2008) Calibrating PAGER ("Prompt Assessment of Global Earthquakes for Response") Ground Shaking and Human Impact estimation using worldwide earthquake datasets: Collaborative Research with USGS and the Swiss Seismological Service, NEHRP Final Report 06HQGR0062.

Dreger, D., and A. Kaverina (2000). Seismic remote sensing for the earthquake source process and near-source strong shaking: A case study of the October 16, 1999 hector mine earthquake, Geophys. Res. Lett., v. 27, p. 1941–1944.

Ebel J. and D. J. Wald (2003). Bayesian Estimations of Peak Ground Acceleration and 5% Damped Spectral Acceleration from Modified Mercalli Intensity Data, Earthquake Spectra, v. 19, no. 3, p. 511–530.

EPRI (2003). CEUS Ground Motion Project: Model Development and Results, EPRI Report 1008910, EPRI, Palo Alto, CA, 105 pp.

Goda, K. and H. P. Hong (2008). Spatial Correlation of Peak Ground Motions and Response Spectra, Bull. Seism. Soc. Am., v. 98, p. 354–365.

Hok, S. and D. J. Wald (2003). Spatial Variability of Peak Strong Ground Motions: Implications for ShakeMap Interpolations, EOS. Trans., AGU, v. 84, no. 46, p. F1121.

Jones, L., R. Bernknopf, S. Cannon, D. A. Cox, L. Gaydos, J. Keeley, M. Kohler, H. Lee, D. Ponti, S. Ross, S. Schwarzbach, M. Shulters, W. Ward, and A. Wein (2007). Increasing Resiliency to Natural Hazards: A Strategic Plan for the Multi-Hazards Demonstration Project in Southern California: U. S. Geological Survey Open File Report 2007–1255.

Lin, K.-W., D. J. Wald, B. C. Worden, and A. F. Shakal (2005). Quantifying CISN ShakeMap Uncertainty, CSMIP '05 Seminar on the Utilization of Strong Motion Data.

Luco, N, and E. Karaka (2007). Extending the USGS National Seismic Hazard Maps and ShakeMaps to probabilistic building damage and risk maps, Proceedings of the 10th Int'l Conf. on Applications of Statistics and Probability in Civil Engineering.

National Institute of Building Sciences and Federal Emergency Management Agency (NIBS and FEMA), 2003, Multi-hazard Loss Estimation Methodology, Earthquake Model, HAZUS®MH Technical Manual, Federal Emergency Management Agency, Washington, DC, 690 pp.

Scherbaum, F., J. Schmedes, and F. Cotton (2004a). On the conversion of source-to-site measures for extended earthquake source models, Bull. Seism. Soc. Am., v. 94, p. 1053–1069.

Scherbaum, F., F. Cotton, and P. Smit (2004b). On the use of response spectral-reference data for the selection and ranking of ground-motion models for seismic-hazard analysis in regions of moderate seismicity: The case of rock motion, Bull. Seism. Soc. Am., v. 94, p. 2164–2185.

Wald, D. J., K. Lin, K. Porter, and L. Turner (2008). ShakeCast: Automating and Improving the Use of ShakeMap for Post-Earthquake Decision-Making and Response": Earthquake Spectra, in press.

Wald, D. J., and T. I. Allen (2007). Topographic slope as a proxy for seismic site conditions and amplification: Bull. Seism. Soc. Am., v. 97, p. 1379–1395.

Wald, D. J., Earle, P. S., Lin, K., Quitoriano, V., and Worden, B. C. (2006). Challenges in rapid ground motion estimation for the prompt assessment of global urban earthquakes: Bull. Earthq. Res. Inst., v. 81, p. 275–283.

Wald, D. J., B. C. Worden, V. Quitoriano, and K. L. Pankow (2005). ShakeMap Manual: Users Guide, Technical Manual, and Software Guide, USGS Techniques and Methods 12–A1, 128 pp. http://pubs.usgs.gov/tm/2005/12A01/

Wald, D. J., V. Quitoriano, T. H. Heaton, and H. Kanamori (1999). Relationship between Peak Ground Acceleration, Peak Ground Velocity, and Modified Mercalli Intensity in California, Earthquake Spectra v. 15, p. 557–564.

Wald, D. J., V. Quitoriano, T. H. Heaton, H. Kanamori, C. W. Scrivner, and B. C. Worden (1999). TriNet "ShakeMaps": Rapid generation of peak ground-motion and intensity maps for earthquakes in southern California, Earthquake Spectra, v. 15, p. 537–556.

Wald, D. J., and T. H. Heaton, and K. W. Hudnut (1996). Rupture history of the 1994 Northridge, California earthquake from strong-motion, GPS, and leveling data, Bull. Seism. Soc. Am., v. 86, p. S49–S70.

Wills, C. J., M. Petersen, W. A. Bryant, M. Reichle, G. J. Saucedo, S. Tan, G. Taylor, and J. Treiman (2000). A site-conditions map for California based on geology and shear-wave velocity, Bull. Seism. Soc. Am. v. 90, p. S187–S208